Coordination and Dehydrogenation of PH_3 by 23 Transition Metal Ions in the Gas Phase: FTICR Experiments and Density Functional Interpretations

Hugh Harris, Keith Fisher, and Ian Dance*

School of Chemistry, University of New South Wales, Sydney, NSW 2052, Australia

Received June 4, 2001

The reactions of 23 transition metal ions $M^+_{(g)}$ with phosphane (PH_3) have been investigated using Fourier transform ion cyclotron resonance spectrometry. Two main reaction pathways are observed, sequential dehydrogenation of multiple (up to nine) phosphane molecules, and addition of multiple (up to four) phosphane molecules. The addition and dehydrogenation reaction pathways are, for the most part, mutually exclusive for a particular metal. Dehydrogenation of phosphane is observed for metal ions toward the lower left of the transition block, and the addition process is predominant toward the top right. The dehydrogenation process is considerably faster than the addition, and sequentially produces the species MPH^+, MP_2^+, MP_3H^+, MP_4^+, etc. Density functional calculations were used to evaluate collision trajectories, reaction mechanisms, structures of intermediates (including a number of $MoP_xH_y^+$ species), and to identify the factors determining whether each metal reacts by dehydrogenation or addition. Insertion of M^+ into P−H bonds is calculated to be a barrierless, exergonic process for only those metals which are observed to dehydrogenate phosphane molecules. A reaction mechanism involving the transfer of H atoms from P to M followed by the elimination of H_2 from M is profiled for Ru. The energetic origins of the metal influence on reaction type have been traced to the energy changes for the first stage migration of H from P to M. These experimental and theoretical results should be valuable in applications where $PH_{3(g)}$ is used in the generation of bulk and surface materials involving metal phosphides.

Introduction

In this paper, we describe the reactions of 23 transition metal ions M^+ with phosphane PH_3 in the gas phase, under Fourier transform ion cyclotron resonance (FTICR) conditions. Using density functional calculations, we provide an interpretation of key aspects of the reaction directions and mechanisms, and describe the structures of products and intermediates. There are two principal and largely independent reaction types, (1) coordinative addition of PH_3 and (2) dehydrogenation of PH_3 with elimination of H_2 and formation of metal phosphides. Both of these types of reactions can be repeated, building series of products.

There are several contexts for this research. One concerns the reactions of $M^+_{(g)}$ with other small binary hydrides XH_n from groups 14, 15, and 16, particularly CH_4, SiH_4, NH_3, OH_2, and SH_2, which surround PH_3 in the periodic table. The variables in this context are: (a) whether the reactant XH_n is a Lewis base, allowing coordinative reactions at X as well as reaction of M with X−H bonds; (b) the characteristics of M reflected in its position in the periodic table; and (c) whether X is first period (C, N, O) or larger. The most studied reactant is CH_4,[1] largely for reasons of interest in the activation of hydrocarbons, and these accumulated results provide information about variable (b), the characteristics of the metal. Methane reacts exothermically with all third row transition metals in groups 4−11 except Hf^+, Re^+, and Au^+,[2] predominantly by facile dehydrogenation for Ta^+, W^+, Os^+, Ir^+, and Pt^+. Hf^+ and Re^+ react endothermically with methane.[3] Zr is the only second row transition metal reported to react with methane in an exothermic dehydrogenation.[4] No first row metals are observed to dehydrogenate methane exothermically, but endothermic dehydrogenation is reported for Ti^+, V^+, and Cr^+.[5] For variable (c), SiH_4 is more reactive than CH_4, being exothermically dehydrogenated by many third, second, and first series transition metals,[6] but not by Cr^+, Fe^+, V^+,[7] or Mn^+.[8] Much thermochemical data has been accumulated for these systems.[9]

The group 15 and 16 hydrides are Lewis bases, with an obvious mechanism for coordinative addition. With ammonia,

(1) Eller, K.; Schwarz, H. *Chem. Rev.* **1991**, *91*, 1121−1177.
(2) Irikura, K. K.; Beauchamp, J. L. *J. Am. Chem. Soc.* **1991**, *113*, 2769−2770.
(3) Irikura, K. K.; Beauchamp, J. L. *J. Phys. Chem.* **1991**, *95*, 8344−8351.
(4) (a) Ranasinghe, Y. A.; MacMahon, T. J.; Freiser, B. S. *J. Phys. Chem.* **1991**, *95*, 7721−7726. (b) Tolbert, M. A.; Beauchamp, J. L. *J. Am. Chem. Soc.* **1986**, *108*, 7509−7517. (c) Tolbert, M. A.; Mandich, M. L.; Halle, L. F.; Beauchamp, J. L. *J. Am. Chem. Soc.* **1986**, *108*, 5675−5683.
(5) (a) Freas, R. B.; Ridge, D. P. *J. Am. Chem. Soc.* **1980**, *102*, 7129−7131. (b) Halle, L. F.; Armentrout, P. B.; Beauchamp, J. L. *J. Am. Chem. Soc.* **1981**, *103*, 962−963. (c) Peake, D. A.; Gross, M. L.; Ridge, D. P. *J. Am. Chem. Soc.* **1984**, *106*, 4307−4315. (d) Jackson, T. C.; Carlin, T. J.; Freiser, B. S. *J. Am. Chem. Soc.* **1986**, *108*, 1120−1126. (e) Georgiadis, R.; Armentrout, P. B. *J. Phys. Chem.* **1988**, *92*, 7067−7074.
(6) (a) Azzaro, M.; Breton, S.; Decouzon, M.; Geribaldi, S. *Rapid Commun. Mass Spectrom.* **1992**, *6*, 306−307. (b) Decouzon, M.; Gal, J.-F.; Geribaldi, S.; Rouillard, M.; Sturla, J.-M. *Rapid Commun. Mass Spectrom.* **1989**, *3*, 298299. (c) Kickel, B. L.; Armentrout, P. B. *J. Am. Chem. Soc.* **1995**, *117*, 4057−4070. (d) Ferhati, A.; McMahon, T. B.; Ohanessian, G. *J. Am. Chem. Soc.* **1996**, *118*, 5997−6009. (e) Irikura, K. K.; Beauchamp, J. L. *J. Am. Chem. Soc.* **1989**, *111*, 75−85. (f) Kang, H.; Jacobson, D. B.; Shin, S. K.; Beauchamp, J. L.; Bowers, M. T. *J. Am. Chem. Soc.* **1986**, *108*, 5668−5675. (g) Kickel, B. L.; Armentrout, P. B. *J. Phys. Chem.* **1995**, *99*, 2024−2032.
(7) Kang, H.; Jacobson, D. B.; Shin, S. K.; Beauchamp, J. L.; Bowers, M. T. *J. Am. Chem. Soc.* **1986**, *108*, 5668−5675.
(8) Kickel, B. L.; Armentrout, P. B. *J. Phys. Chem.* **1995**, *99*, 2024−2032.
(9) Rodgers, M. T.; Armentrout, P. B. *Mass Spectrom. Rev.* **2000**, *19*, 215−247.

10.1021/ic0105821 CCC: $20.00
Published on Web 11/17/2001

first row transition metals V^+ to Cu^+ form adducts $[M(NH_3)_x]^+$ detected under flowing afterglow conditions,[10] while under FTICR conditions, dehydrogenation is dominant for Sc^+, Ti^+, V^+, Y^+, Zr^+, Nb^+, La^+, Ta^+, and Os^+.[6e,11] Ammonia enclosure of metal ions has been studied.[12] Thermochemical and kinetic data for addition and dehydrogenation are available for Sc^+ and Ti^+,[13] V^+,[14] Co^+, Ni^+ and Cu^+.[15] The reactions of phosphane (PH_3) have been reported only for Si^+,[16] Cr^+,[17] Pt^+,[18] FeO^+,[19] and P^+.[20] The $Cr^+ + PH_3$ mixture yielded only slow addition,[17] while the $Pt^+ + PH_3$ reaction underwent sequential dehydrogenations, leading to PtP_6^+.[18] The reactions of first transition series M^+ with water have been studied in detail both experimentally and theoretically.[21]

The subject of this paper, PH_3, has been the least studied, and yet it is potentially significant as a gaseous reactant in the formation of metal phosphide materials with desirable electronic properties. These applications are another significant context of this research. Dehydrogenation is widely used to generate new species.[22] Metal vapor deposition in a PH_3 matrix has been reported,[23] as have investigations of PH_3 on metal surfaces.[24]

Therefore, we report here on the reactions of 23 of the 29 nonradioactive transition metal ions, all under the same FTICR conditions, with the neglected, but significant, reactant PH_3. The objective is to provide an overall understanding. We have previously reported a similar comparative investigation of 29 transition metals[25] and the lanthanide metals[26] as $M^+_{(g)}$ reacting with $S_{8(g)}$. We interpret our experimental data using density functional calculations of the possible structures of intermediate products and some transition states, reaction mechanisms, and calculations relating to the differentiation between addition and dehydrogenation.

Experimental Methods

All experiments were performed in a Bruker Fourier Transform Ion Cyclotron Resonance (FTICR) mass spectrometer, with a 4.7 T magnet. The metal sample, located at one end of the FTICR cell, was ablated with a pulse from a Nd:YAG laser at 1064 nm, in the presence of a mixture of 10% PH_3 in argon. A 2 s delay after ablation was employed to allow collisions to remove excess kinetic and electronic energy from the ablation products. The M^+ cation was then selected by rejection of all other ions, and reaction with the PH_3 was allowed to continue for variable periods up to 1 min. Pressures of the gas mixture were between 1×10^{-7} and 5×10^{-7} Torr. Adventitious water generated some products containing oxygen, but these did not interfere with the monitoring of the $M^+ + PH_3$ reactions. The precision of the experiments allowed selection of single metal isotopes and precise identification of the number of H atoms in product ions. Selected products of the $M^+ + PH_3$ reactions were accelerated in the cell and allowed to collide with argon, causing partial fragmentation (collision induced dissociation, CID). This use of CID enabled resolution of mass ambiguities such as PH = 32 Da = O_2. The apparatus and methods have been described previously.[26]

Computational Methods

Density functional calculations used the methodology and numerical basis sets of the program DMol,[27] versions DMol400 and DMol3.[28] The results reported in this paper were generated within the spin-unrestricted formalism using the Becke exchange functional[29] and the Lee−Yang−Parr correlation functional.[30] The nonlocal corrections were applied post-SCF. The numerical basis sets (type DNP in DMol) for element E were double numerical, augmented with polarization functions for all atoms including hydrogen, and obtained by the orthogonalized combination of the solutions of the DF equations for E, E^{2+}, and E with excitation of one valence electron. Calculations involving first and second row metals treat core atomic orbitals for all atoms as noninteracting, while calculations involving third row metals (with DMol3) included relativistically corrected atomic potentials and no freezing of core orbitals. As validation, our methodology yielded 35 kcal mol^{-1} for the inversion barrier of PH_3, which is compared with values of 34−35 kcal mol^{-1} obtained using other methods, and 32 kcal mol^{-1} obtained experimentally.[23c]

Geometry optimization was effected by minimization of the total energy. Bond orders were calculated using the Mulliken partitioning method,[31] as implemented in DMol. To locate transition states and determine activation energies, a reaction path following (RPF) methodology was employed. Automatic gradient-based transition state searches generally provided little valuable information, even close to the RPF transition state, due to the configurational freedom of these coordinatively unsaturated molecules and the flat gradients, particularly with respect to the position of H atoms on M. Our procedure started by testing various structures near a postulated transition state until two structures were found, one (**P**), which optimized without constraints to the product, and one (**R**), which optimized to the reactant. The geometrical average of these two structures (**A1**) was then optimized, resulting in the geometry of either **P** or **R**. The geometrical average of **A1** and the member of the set **P**, **R** to which **A1** does not optimize is the next estimate of the transition state, **A2**. This hill-climbing algorithm is repeated until two consecutive geometrically averaged structures (**Ax** and **Ax + 1**) are identical. The performance of DF calculations on predicting transition state structures and energies has been validated previously.[32]

(10) Marinelli, P. J.; Squires, R. R. *J. Am. Chem. Soc.* **1989**, *111*, 4101−4103.
(11) Buckner, S. W.; Gord, J. R.; Freiser, B. S. *J. Am. Chem. Soc.* **1988**, *110*, 6606−6612.
(12) (a) Sato, H.; Matsuzaki, A.; Nishio, S.; Ito, O.; Furukawa, K.; Kawasaki, T. *J. Phys. Chem.* **1998**, *108*, 3940−3954. (b) Milburn, R. K.; Baranov, V. I.; Hopkinson, A. C.; Bohme, D. K. *J. Phys. Chem. A* **1998**, *102*, 9803−9810.
(13) Clemmer, D. E.; Sunderlin, L. S.; Armentrout, P. B. *J. Phys. Chem.* **1990**, *94*, 3008−3015.
(14) Clemmer, D. E.; Sunderlin, L. S.; Armentrout, P. B. *J. Phys. Chem.* **1990**, *94*, 208−217.
(15) Clemmer, D. E.; Armentrout, P. B. *J. Phys. Chem.* **1991**, *95*, 3084−3090.
(16) Hrusak, J.; Schroder, D.; Schwarz, H.; Iwata, S. *Bull. Chem. Soc. Jpn.* **1997**, *70*, 777−787.
(17) Mazurek, W.; Schwarz, H. *Inorg. Chem.* **2000**, *39*, 5586−5590.
(18) Bronstrup, M.; Schroder, D.; Schwarz, H. *Organometallics* **1999**, *18*, 1939−1948.
(19) Bronstrup, M.; Schroder, D.; Schwarz, H. *Chem. Eur. J.* **1999**, *5*, 1176−1185.
(20) Antoniotti, P.; Operti, L.; Rabezzana, R.; Splendore, M.; Tonachini, G.; Vaglio, G. A. *J. Chem. Phys.* **1997**, *107*, 1491−1500.
(21) Irigoras, A.; Elizalde, O.; Silanes, I.; Fowler, J. E.; Ugalde, J. M. *J. Am. Chem. Soc.* **2000**, *122*, 114−122.
(22) Chen, Z. Y.; Walder, G. J.; Castleman, A. W. *Phys. Rev. B*: **1994**, *49*, 2739−2752.
(23) (a) Bowmaker, G. A. *Aust. J. Chem.* **1978**, *31*, 2549−2553. (b) Trabelsi, M.; Loutellier, A. *J. Mol. Struct. (THEOCHEM)* **1978**, *43*, 151−157. (c) Himmel, H.-J.; Downs, A. J.; Greene, T. M. *Inorg. Chem.* **2001**, *40*, 396−407.
(24) (a) Hegde, R. I.; Tobin, J.; White, J. M. *J. Vac. Sci. Technol.* **1985**, *3*, 339−345. (b) Hegde, R. I.; White, J. M. *Surf. Sci.* **1985**, *157*, 17−28. (c) Mitchell, G. E.; Henderson, M. A.; White, J. M. *Surf. Sci.* **1987**, *191*, 425−447.
(25) Dance, I. G.; Fisher, K. J.; Willett, G. D. *Inorg. Chem.* **1996**, *35*, 4177−4184.
(26) (a) Fisher, K.; Dance, I.; Willett, G. *J. Chem. Soc., Dalton Trans.* **1998**, 975−980. (b) El Nakat, J. H.; Fisher, K. J.; Dance, I. G.; Willett, G. D. *Inorg. Chem.* **1993**, *32*, 1931−1940. (c) Dance, I. G.; Fisher, K. J.; Willett, G. D. *Inorg. Chem.* **1996**, *35*, 4177−4184. (d) Greenwood, P. F.; Dance, I. G.; Fisher, K. J.; Willett, G. D. *Inorg. Chem.* **1998**, *37*, 6288−6294.
(27) (a) Delley, B. *New J. Chem.* **1992**, *16*, 1103−1107. (b) Delley, B.; Wrinn, M.; Lüthi, H. P. *J. Chem. Phys.* **1994**, *100*, 5785−5791. (c) Delley, B. *J. Chem. Phys.* **1990**, *92*, 508−517. (d) Delley, B. *J. Chem. Phys.* **1991**, *94*, 7245−7250.
(28) MSI http://www.msi.com.
(29) Becke, A. D. *Phys. Rev. A* **1988**, *38*, 3098.
(30) Lee, C.; Yang, W.; Parr, R. G. *Phys. Rev. B*: **1988**, *37*, 785−789.
(31) Mulliken, R. S. *J. Chem. Phys.* **1955**, *23*, 1833−1846.

Results

Observed Reactions of M^+ with PH_3. General Patterns. For the twenty-three naturally occurring transition metals investigated, two distinct reaction pathways with phosphane were observed (except for unreactive Mn^+ and Fe^+), namely coordinative addition and dehydrogenation. The coordinative reaction, eq 1, can occur as a series of additions, as represented by the general equation (1′)

$$M^+ + PH_3 \rightarrow [MPH_3]^+ \quad (1)$$

$$[M(PH_3)_x]^+ + PH_3 \rightarrow [M(PH_3)_{x+1}]^+ \quad (1')$$

The first stage of dehydrogenation is shown in eq 2, eliminating one molecule of H_2. This can be followed by a second dehydrogenation stage with another molecule of phosphane, eq 3, eliminating two molecules of H_2. These processes can continue further, according to the general eqs 2′ and 3′ for the sequential processes.

$$M^+ + PH_3 \rightarrow [MPH]^+ + H_2 \quad (2)$$

$$[MPH]^+ + PH_3 \rightarrow [MP_2]^+ + 2H_2 \quad (3)$$

$$[MP_x]^+ + PH_3 \rightarrow [MP_{x+1}H]^+ + H_2 \quad (2')$$

$$[MP_{x+1}H]^+ + PH_3 \rightarrow [MP_{x+2}]^+ + 2H_2 \quad (3')$$

Representative spectra for metals reacting via each pathway are shown in Figure 1. A general result is that dehydrogenation is much faster than addition. After 100 s of reaction time, Cu^+ has only partly reacted by addition and is still the most abundant ion in the spectrum (Figure 1 (a)). In contrast, after only 15 s at the same phosphane pressure, Os^+ has reacted almost completely by dehydrogenation (Figure 1 (b)). The higher efficiency of the dehydrogenation process, in comparison with addition, leads to the possibility that addition products may be masked by the presence of more abundant dehydrogenation products. The only exceptions to the generalization about relative rates of addition and dehydrogenation occur with Au^+ and Pd^+, which react with PH_3 by both reaction types at similar rates, but yield only a short series of products. Representative reaction profiles for Ru, Rh, Ir, and Au are given in Figure 2. The sequence of dehydrogenation reactions according to cycles of coupled reactions 2′ and 3′ are clear for Ru, Rh, and Ir, which reach $[RuP_6]^+$, $[RhP_4]^+$, and $[IrP_6]^+$. For Au^+, the first stage of dehydrogenation occurs at similar rate to that of the other metals, and the first addition process forming $[AuPH_3]^+$ follows soon after. The dual reaction types are observed for Au^+ because the addition is unusually fast.

A complete listing of observed species for all metals is provided in Table 1. Figure 3 summarizes the reaction types for all metals. Two metals, Mn^+ and Fe^+, show no evidence of any reaction, even after 50 s. For the metals that are observed to react via addition only, namely Cr^+, Co^+, Ni^+, Cu^+, and Ag^+, the M^+ ion is still the most abundant in the spectrum after 100s, and only trace amounts of products are observed for Ag^+ and Cr^+. In contrast, of the dehydrogenating metals, only the slowest reacting metal ions, V^+ and Mo^+, show relative abundances for the metal ion of more than 50% after 10 s. A recent investigation of $Cr^+ + PH_3$ also found that only very slow addition occurred, and this was attributed to the ^6S ground state of Cr^+.[17]

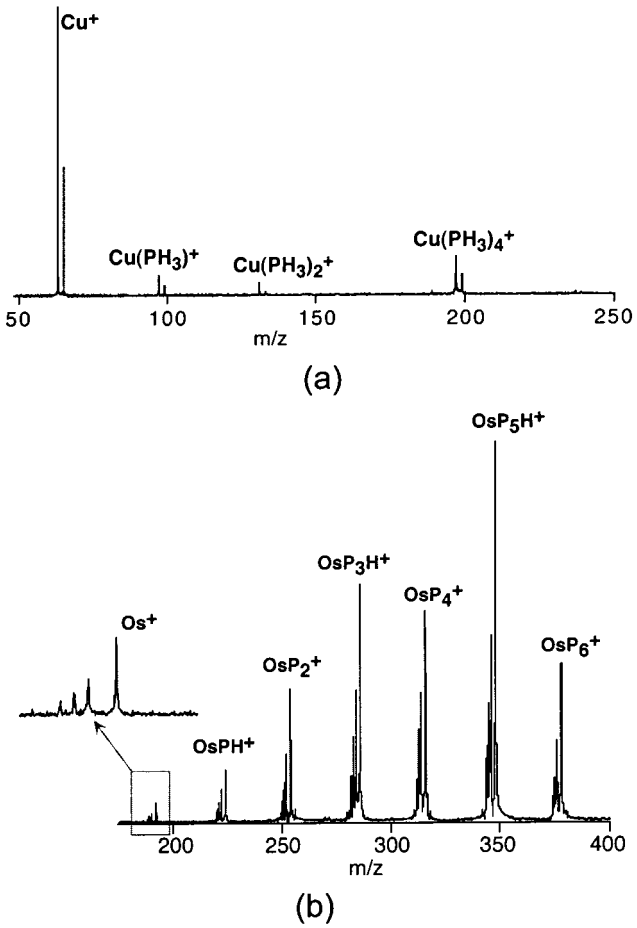

Figure 1. (a) Mass spectrum of the products of reaction of Cu^+ with PH_3 after 100 s. (b) Mass spectrum of the products of reaction of Os^+ with PH_3 after 15 s.

The reaction rates of the M^+ ions are reported (Table 2) relative to the rate for Zr^+, which is effectively the collision controlled rate. Rate measurements found that Zr^+ reacted with PH_3 2.6 times faster than the rate of charge transfer between Ar^+ (generated by EI) and PH_3, and since charge transfer is believed to occur at close to the collision rate, it is concluded that the reaction of Zr^+ with PH_3 is effectively at the collisional limit. With the exceptions of Pd^+ (which dehydrogenates slowly) and Au^+ (which adds quickly), the general conclusion from Table 2 is that dehydrogenation approaches the collision rate for many metals, but that addition is approximately two orders of magnitude less efficient.

Extent of Reaction. The very slow addition of PH_3 to Cr^+ yields only the monoadduct; for Ag^+ and Au^+, the bis adducts are observed, while for the late first series metals Co^+, Ni^+ and Cu^+, three, four, and maybe five PH_3 are added (Table 1). We note that co-condensation of these metal atoms with PH_3 in Kr matrixes leads to the adducts $Cu(PH_3)_n$, $n = 1, 2, 3$,[23] and $Ni(PH_3)_n$, $n = 1, 4$. We observe three single addition products, VPH_3^+, $ZrPH_3^+$, and $HfPH_3^+$, for metals which otherwise react by dehydrogenation.

The sequential dehydrogenations usually occur for at least four cycles (each cycle being 2′ + 3′), while the largest number of cycles observed was nine, with Os^+. Mo^+ clearly proceeds through eight cycles of dehydrogenation, and W^+ proceeds through seven (see Table 1). The only other reaction of M^+

(32) (a) Ziegler, T. *Chem. Rev.* **1991**, *91*, 651−667. (b) Fan, L.; Ziegler, T. In *Density Functional Theory of Molecules, Clusters and Solids*; Ellis, D. E., Ed.; Kluwer: Dordrecht, 1995; pp 67−95. (c) Han, Y.; Deng, L.; Ziegler, T. *J. Am. Chem. Soc.* **1997**, *119*, 5939−5945.

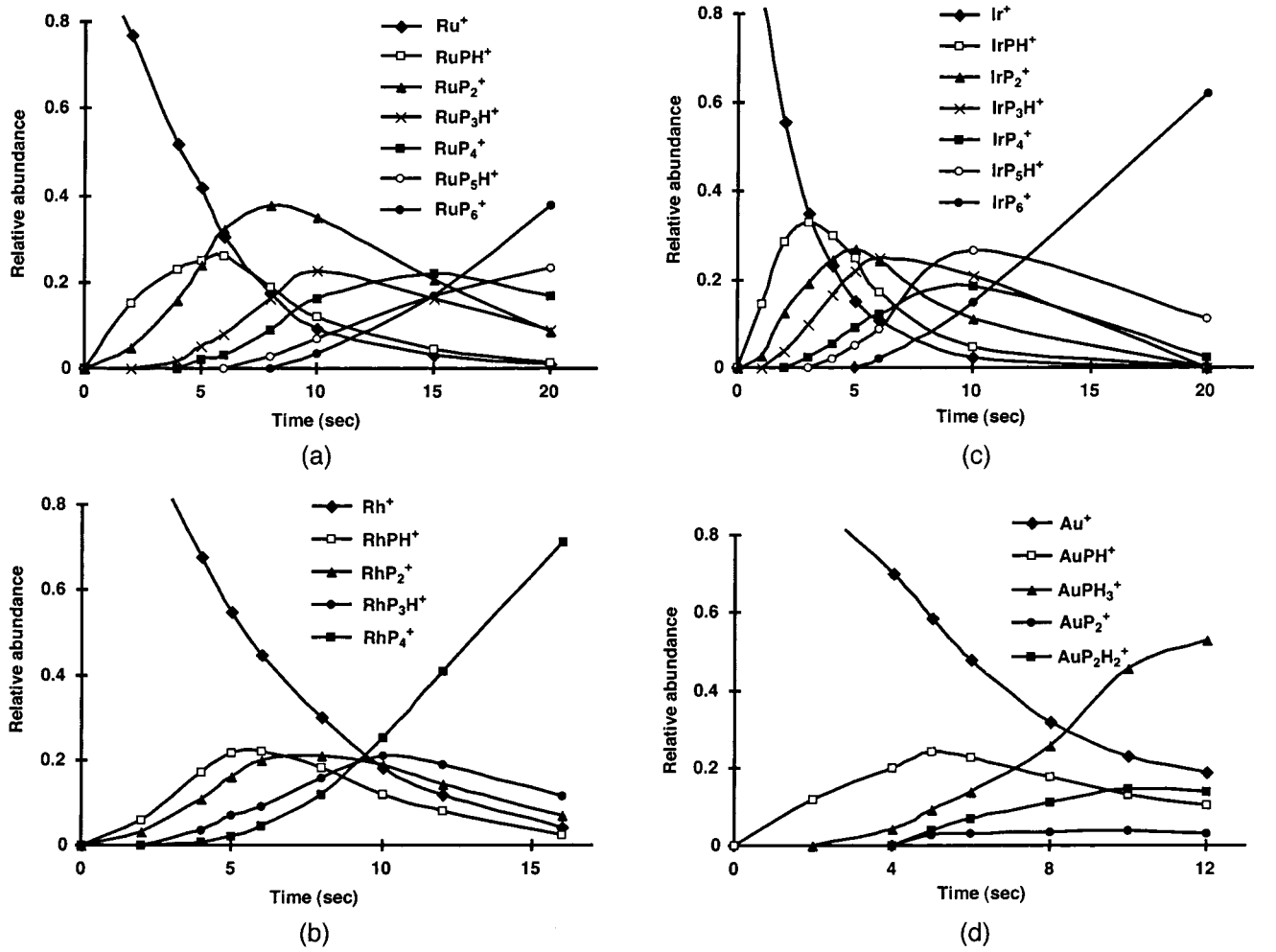

Figure 2. Reaction profiles for the reaction of (a) Ru, (b) Rh, (c) Ir, and (d) Au with phosphane in argon. All reactions were performed with background gas at 1×10^{-7} Torr, except Ir at 2×10^{-7} Torr.

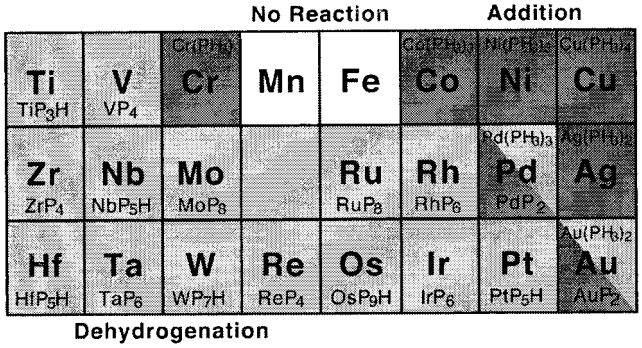

Figure 3. Classification of the transition metals based on their experimental reaction behavior as $M^+_{(g)} + PH_{3(g)}$. The main reaction pathways are dehydrogenation of PH_3, for metals on the lower left (light gray), and PH_3 addition, for metals on the upper right (dark gray). Mn and Fe are unreactive. Au and Pd show both pathways. The formulas in each box represent the maximum extent of addition (top of the box) or dehydrogenation (bottom of the box).

with PH_3 reported in the literature was with Pt^+,[18] where the reaction proceeded to PtP_6^+ (we observe five cycles); the rate constants were measured, and it was determined that dehydrogenations of type (3′) eliminating $2H_2$ were faster than those of type (2′).[18]

Metals ions which dehydrogenate PH_3 normally yield products which contain either one or zero H atoms, according to equations (2′) or (3′). However, some minor products occur for Mo, Nb, Re, and Au which contain two or more H atoms.

Some of the products observed could represent a combination of the dehydrogenation and addition pathways, such as $[NbP_3H_3]^+$ and $[MoP_3H_3]^+$ (possibly $[MP_2(PH_3)]^+$), $[NbP_5H_3]^+$ and $[MoP_5H_3]^+$ (ie $[MP_4(PH_3)]^+$), and $[MoP_7H_3]^+$ (ie $[MP_6(PH_3)]^+$) (Table 1). There are also a few species observed that seem likely to be products of partial completion of reaction (3′) above, for example $[TaP_4H_2]^+$ and $[ReP_4H_2]^+$, among several others listed in Table 1. Still, other species, such as $[MoP_7H_5]^+$, seem likely to be formed through a combination of addition and partial dehydrogenation. The previous study of Pt^+ with PH_3[18] also observed parallel reaction types.

Species with an even number of H atoms are rare. Ions MPH_2^+ for M = V, Zr, and Hf could be regarded as evidence of loss of H rather than H_2 in reaction 2, but are more likely to be due to elimination of one rather than two H_2 in reaction 3.

Collision-induced dissociation (CID) experiments were performed on a number of product ions, and the results are presented in Table 3. $[MH]^+$ was observed for M = Ti, Zr, Nb, Hf, Ta, W, Sb, Pt, Ir, and Os via CID of species containing P and H, but not O. The formation of $[MH]^+$ in these CID experiments supports the assigned composition of products where there could have been ambiguity between $[MO_2]^+$ or $[MPH]^+$ due to the mass similarity of these two species.

There is a clear pattern in the periodicity of the reactivity of the metals, as shown in Figure 3. Metals M^+ to the top right undergo addition and no dehydrogenation, and $[Cu(PH_3)_4]^+$ is the largest addition product. In contrast, metals to the lower

Table 1. Cationic Products Observed by Reaction of M^+(g) with PH_3 in the FTICR Cell[a]

M	oxygen-free products observed
Ti^+	$TiPH^+$, $TiPH_3^+$, TiP_2^+, TiP_3H^+
V^+	VPH^+, VPH_2^+, VPH_3^+, VP_2^+, VP_3H^+, VP_4^+
Cr^+	$CrPH_3^+$ only
Mn^+	No reaction even after 50s
Fe^+	No reaction even after 50s
Co^+	$Co(PH_3)_x^+$ for $x = 1-3$ also trace CoP_2^+
Ni^+	$Ni(PH_3)_x^+$ for $x = 1-3$ (all weak)
Cu^+	$Cu(PH_3)_x^+$ for $x = 1, 2, 4, (5)$
Zr^+	$ZrPH^+$, $ZrPH_2^+$, $ZrPH_3^+$, ZrP_2^+, $\{ZrP_2H^+\}$, ZrP_3H^+, ZrP_4^+
Nb^+	$NbPH^+$, NbP_2^+, NbP_3H^+, $NbP_3H_3^+$, NbP_4^+, $NbP_4H_2^+$, NbP_5H^+, $NbP_5H_3^+$
Mo^+	$MoPH^+$, MoP_2^+, MoP_3H^+, $MoP_3H_3^+$, MoP_4^+, $MoP_4H_2^+$, MoP_5H^+, $MoP_5H_3^+$, MoP_6^+, $MoP_6H_{2,4}^+$, MoP_7H^+, $MoP_7H_{3,5}^+$, MoP_8^+, $MoP_8H_4^+$
Ru^+	$RuPH^+$, RuP_2^+, RuP_3H^+, RuP_4^+, RuP_5H^+, RuP_6^+, $\{RuP_7H^+\}$, $\{RuP_8^+\}$
Rh^+	$RhPH^+$, RhP_2^+, RhP_3H^+, RhP_4^+, $\{RhP_5H^+\}$, $\{RhP_6^+\}$
Pd^+	$Pd(PH_3)_x^+$ for $x = 1-3$, PdP_2^+
Ag^+	Trace amounts of $Ag(PH_3)^+$ and $Ag(PH_3)_2^+$
Hf^+	$HfPH^+$, $HfPH_2^+$, $HfPH_3^+$, HfP_2^+, HfP_3H^+, HfP_4^+, HfP_5H^+
Ta^+	$TaPH$, TaP_2^+, TaP_3H^+, TaP_4^+, $TaP_4H_2^+$, TaP_5H^+, TaP_6^+
W^+	WPH, WP_2^+, WP_3H^+, WP_4^+, WP_5H^+, WP_6^+, WP_7H^+
Re^+	$RePH^+$, ReP_2^+, $ReP_2H_2^+$, ReP_3H^+, $ReP_4H_2^+$
Os^+	$OsPH$, OsP_2^+, OsP_3H^+, OsP_4^+, OsP_5H^+, OsP_6^+, OsP_7H^+, OsP_8^+, OsP_9H^+
Ir^+	$IrPH^+$, IrP_2^+, IrP_3H^+, IrP_4^+, IrP_5H^+, IrP_6^+, $\{IrP_7H^+\}$, $\{IrP_8^+\}$
Pt^+	$PtPH^+$, PtP_2^+, PtP_3H^+, PtP_4^+, PtP_5H^+
Au^+	$AuPH^+$, $AuPH_3^+$, AuP_2^+, $AuP_2H_2^+$, $Au(PH_3)_2^+$

[a] Species in braces {} are observed only with low intensity, while other species are observed with significant abundance after a specific reaction time (see text).

left undergo the much faster dehydrogenation, and Zr^+ in group 4 is the fastest reacting metal ion. Pd^+ and Au^+ on the border show fast addition which can compete with dehydrogenation.

From this pattern it would be expected that Mn^+ and Fe^+ would undergo addition, but this was not observed; we expect that addition occurs but is too slow for our experiments.

Density Functional Investigations. The experimental results presented above raise a number of questions. What are the structures of the newly observed species? What is the mechanism for dehydrogenation of phosphane molecules? Why is the dehydrogenation process generally much more efficient than addition? Which property of the metal ion determines the reaction pathway? We address these questions using density functional theory.

We first consider the probable structures of the smaller products, $[MPH]^+$, $[MP_2]^+$, and $[MPH_3]^+$, for each of the metals.

Structures of MPH^+. Energy minima for MPH^+ were identified by optimization of three connectivities, **1**, **2**, and **3**; the connectivity M−H−P was not competitive and, therefore, not investigated further. For connectivities **1** and **3**, the H−M−P or M−P−H angle was initially 135°, with the aim of allowing optimization toward linear or orthogonal structures. Starting structures were identical for all metals.

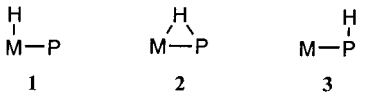

1 **2** **3**

The calculated binding energies for the optimized structures, relative to the most stable structure type for each metal, are presented in Table 4. For all metals, the energy surface with respect to the H−M−P angle in structure **1** of Table 4 is quite flat, with angle variation of 5−10° corresponding to small (0−5 kcal mol^{-1}) energy variations. The low number of local minima in Table 4 indicates that the geometry−energy hypersurfaces for these molecules are not complex. Geometrical properties of the energy minimized structures are presented in Figure 4.

Some periodic trends are noted in the results in Table 4. Bridging hydrogen (**2**) is found to be the most stable arrangement for the early transition series metals, Ti, V, Zr, Nb, and Hf, but is not even a minimum for the majority of remaining

Table 2. Experimentally Observed Reaction Pathway, Rate, and Extent for $M^+ + PH_3$[a]

metal	reaction type	rate, relative to collision rate	no. of abundant products
Ti	dehydrogenation	0.3[b]	2
V	dehydrogenation	0.1[b]	4
Cr	addition	<0.01	0
Mn	none	−	0
Fe	none	−	0
Co	addition	<0.01	0
Ni	addition	<0.01	0
Cu	addition	<0.01	0
Zr	dehydrogenation	1.0[b]	2
Nb	dehydrogenation	0.2[b]	5
Mo	dehydrogenation	0.1	6
Ru	dehydrogenation	0.8	6
Rh	dehydrogenation	0.7	4
Pd	addition	0.01[c]	0
Pd	dehydrogenation	0.01[c]	0
Ag	addition	<0.01	0
Hf	dehydrogenation	0.6[b]	4
Ta	dehydrogenation	0.5[b]	4
W	dehydrogenation	0.4[b]	6
Re	dehydrogenation	0.3[b]	4
Os	dehydrogenation	0.3	6
Ir	dehydrogenation	0.6	6
Pt	dehydrogenation	0.6	4
Au	dehydrogenation	0.5[c]	0
Au	addition	0.5[c]	1

[a] The rate is the depletion rate of M^+ relative to the estimated collision rate (the rate of depletion Zr^+, see text). Rates have been normalized to the same pressure of PH_3. Also tabulated are the numbers of abundant product ions (major peaks at any stage in the reaction) and the total number of product ions in the reaction sequence. [b] Reaction rates include contributions from reaction of the metal ion with water. [c] Rate includes similar contributions from both dehydrogenation and addition processes.

Table 3. Ions Produced in the $M^+ + PH_3$ Reactions Investigated Further by Collision Induced Dissociation (CID), and the Daughter Ions Observed. Species in Braces {} Have Very Low Intensity

parent ion	observed CID daughters
$TiPH^+$	Ti^+, TiH^+
TiP_2^+	TiP^+, Ti^+
VP_2^+	VP^+, V^+
VP_4^+	VP_2^+, VP^+, V^+
$VP_4OH_2^+$	VP_4^+, VP_3OH^+, VP_3^+, $VP_2OH_2^+$, VP_2^+, VP^+, V^+
$ZrPH^+$	Zr^+, ZrH^+
ZrP_2^+	ZrP^+, Zr^+, $\{ZrH^+$, ZrH_2^+, $ZrH_4^+\}$
NbP_2^+	NbP^+, Nb^+
NbP_2O^+	NbP_2^+, $NbPO^+$, NbP^+, Nb^+, NbO^+
NbP_3H^+	NbP_3^+, NbP_2^+, $NbPH^+$, NbP^+, Nb^+, NbH^+
MoP_3OH^+	MoP_3^+, MoP_2^+, $MoPOH^+$, MoP^+, Mo^+, $MoOH^+$
$HfPH^+$	HfH^+, Hf^+
HfP_2^+	HfP^+, Hf^+
$TaPH^+$	Ta^+, TaH^+
$TaPOH^+$	$TaPH^+$, TaO^+, Ta^+
TaP_2^+	TaP^+, Ta^+
WPH^+	WH^+, W^+
WP_2^+	WP^+, W^+
$OsPH^+$	OsH^+, Os^+, $\{OsP^+\}$
OsP_3H^+	OsP_2^+, $\{OsP_2H^+\}$, OsP^+, $\{OsPH^+\}$, OsH^+, Os^+
OsP_4^+	$\{OsP_3^+\}$, OsP_2^+, OsP^+, Os^+
OsP_5H^+	OsP_3H^+, OsP_3^+, OsP_2H^+, OsP_2^+, $OsPH^+$, OsH^+, Os^+

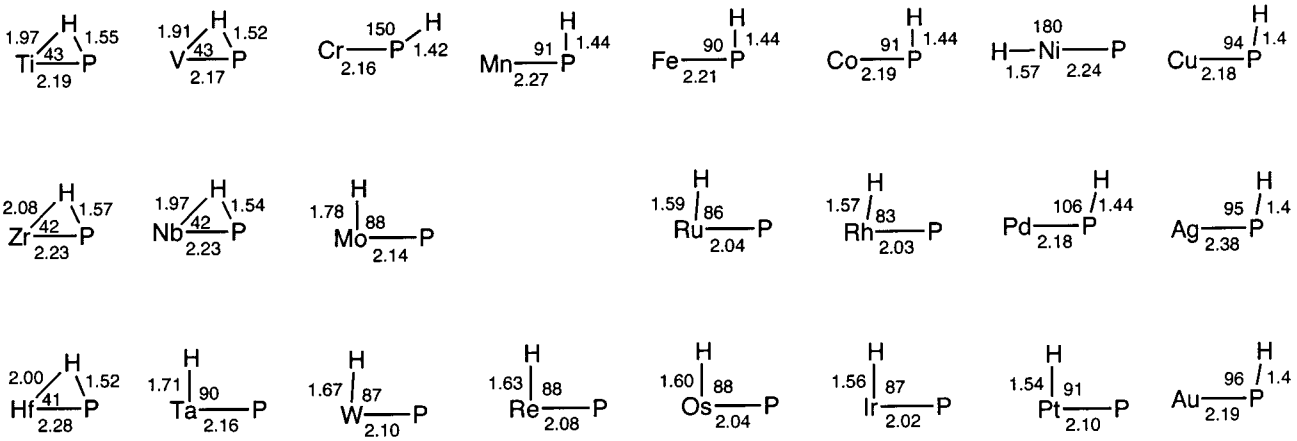

Figure 4. The optimized geometries (Å, °) of MPH^+.

Table 4. Optimized Structures and Relative Energies (kcal mol^{-1}) for Species of Composition MPH^+ [a]

	H M—P **1**	H M—P **2**	H M—P **3**
Ti	⇒	0	3.7 (l)
V	⇒	0	⇐
Cr	22.4	2.4	0
Mn	19.8	⇒	0
Fe	⇒	⇒	0
Co	⇒	⇒	0
Ni	22.7 (linear)	0[b]	37.3
Cu	⇒	⇒	0
Zr	⇒	0	6.7
Nb	4.4	0	5.8 (linear)
Mo	0	1.6	4.0 (linear)
Ru	0	⇐	16.7
Rh	0	⇐	3.4
Pd	19.5	⇒	0
Ag	⇒	⇒	0
Hf	13.9	0	7.4
Ta	0	2.3	12.2 (linear)
W	0	13.8	⇐
Re	0	⇒	21.0
Os	0	⇐	31.1
Ir	0	⇐	24.8
Pt	0	⇐	13.0
Au	31.0	⇒	0

[a] The three columns represent the three starting geometry types; arrows indicate connectivity changes during energy minimization, from the structure with the arrow to that indicated by the direction of the arrow. The numbers are calculated binding energies of minima relative to the most stable geometry (= 0). Optimized structures for connectivities **1** and **3** are not necessarily perpendicular, and in some cases are linear, as marked. [b] $NiPH^+$ with structure **2** dissociates to Ni^+ plus P−H on energy minimization.

metals and reverts to one of the H-terminal structures on optimization. Species with metals toward the right of the transition series tend to favor P−H bonding, particularly in the first series, while species containing mid-series metals favor M−H bonding. Ni is unique, with linear H−Ni−P^+ as the most stable bonded structure, but dissociated Ni^+ plus P−H has lower energy and is formed on optimization of structure **2**.

Table 5. Calculated Relative Energies (kcal mol^{-1}) of Three Structure Types for MP_2^+

M	**4**	M−P−P	P−M−P
Ti	0	49	99
V	0	57	105
Zr	0	55	122
Nb	0	69	125
Mo	0	60	115
Ru	0	26	84

The lowest energy structures of the MPH^+ species are calculated to have HOMO−LUMO gaps of at least 0.5 eV, with the exception of $FePH^+$ with a gap of 0.25 eV. The nondissociated $NiPH^+$ structures, however, have a number of energetically close-lying molecular orbitals at the Fermi level, possibly explaining their calculated instability.

Structures of MP_2^+. The linear geometries P−M−P and M−P−P and the bent P−M−P geometry were tested for MP_2^+ (where M = Ti, V, Zr, Nb, Mo, and Ru). The linear structures were constrained to $C_{\infty v}$ symmetry. Optimization of a bent structure with a P−P distance of 3.3 Å resulted in the spontaneous formation of a P−P bond for all metals tested. This structure, **4**, with the metal bound to the side of a P_2 unit, was found to have the lowest energy for all species considered. The relative energies listed in Table 5 show the favorability for P−P bonding in MP_2^+, as structures without a P−P bond are destabilized by at least 84 kcal mol^{-1} relative to **4**. All of the MP_2^+ lowest energy structures have calculated HOMO−LUMO gaps of at least 0.5 eV, except that of Mo (0.15 eV).

4

Structures and Potential Energy Surfaces of MPH_3^+. The MPH_3^+ composition is observed for 11 of the 23 metals, but it must have at least a transient existence as a collision complex for those metals where it is not observed. Therefore, an understanding of the energy−geometry surface for MPH_3^+ is important to rationalize both its appearance and its instability for different metals. This was modeled by calculating various approaches of M^+ ions toward PH_3, providing information about ground-state structures and about transformations between structures.

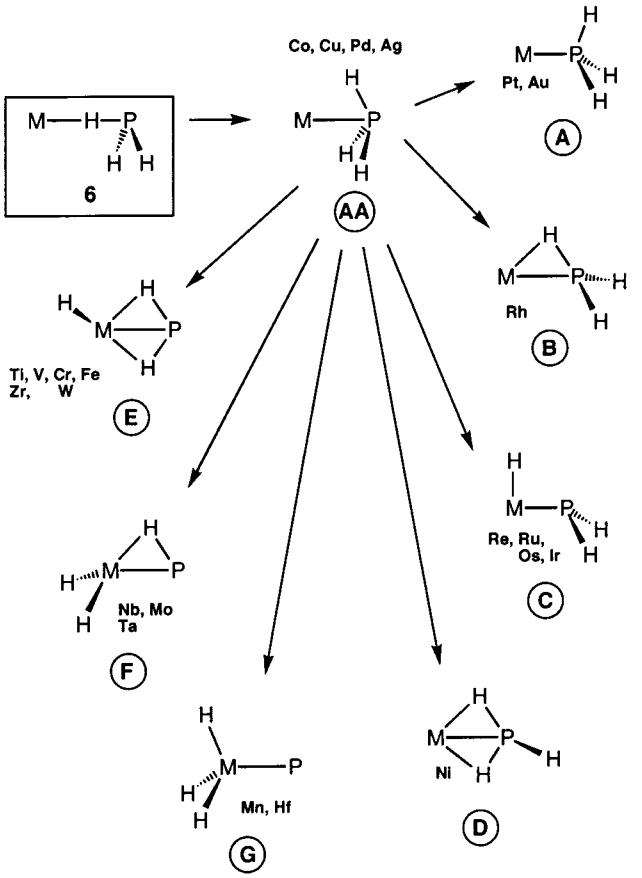

Figure 5. The course of the density functional optimization of $MHPH_2^+$ with structure **6**, for 23 metals. C_s symmetry was imposed for third transition series metals. The final structure for each metal is indicated by the metal symbols near each structure.

For each MPH_3^+ species, two starting structures were considered initially. One, **5**, had the metal atom bound to the phosphorus atom (M−P = 2.0 Å) as an M−PH_3 species with three-fold symmetry, while the other, **6**, had M−H−PH_2 geometry with the metal located as an extension of a P−H vector (M−H = 1.5 Å). The MPH_3^+ structure **5** was constrained to C_{3v} symmetry, and no inversion or dissociation of PH_3 occurred during optimization, indicating that this is a stable binding mode for all metals.

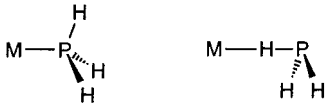

5 **6**

The results of optimization of **6** for all metals are presented in Figure 5. In all cases, the optimization proceeded first to structure **AA**, with approximate C_{3v} symmetry and the metal inside the H_3P cone. However, **AA** is a local minimum only for Co, Cu, Pd, and Ag, and for other metal systems, optimization results in more significant rearrangements. Exergonic inversion of the phosphane (to **A**) is calculated for $PtPH_3^+$ and $AuPH_3^+$, resulting in the M−PH_3 adduct structure already described. For Rh and Ni there is formation of one M−H−P bridge (**B**, Rh) or two M−H−P bridges (**D**, Ni), but no bond breaking. For all of the other metals at least one P−H bond is broken and one terminal M−H bond is formed; barrierless hydrogen atom migration from phosphorus to the metal is calculated to occur for 15 of the 23 species with geometry **6**.

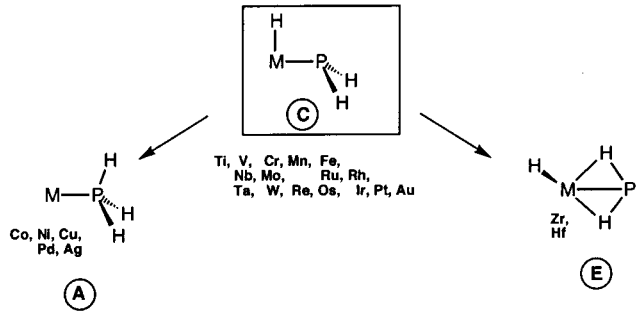

Figure 6. The results of density functional optimization of $HMPH_2^+$ with structure **C** for all 23 metals; C_s symmetry was imposed. The transformations to **A** or **E** for the metals marked are barrierless processes. The metals identified under **C** showed no change in connectivity.

To further explore the surface for H atom migration, we optimized structure **C** for all metals, with the results presented in Figure 6. Barrierless hydrogen atom migration from terminal M−H to terminal P−H was calculated for Co, Ni, Cu, Pd, and Ag, forming **A**, which is fully consistent with the results of Figure 6 and the preference for P−H bonding with these metals. All other metal systems retain their M−H bonding. The formation of structure **E** by Zr occurs in both optimization pathways.

The geometry−energy hypersurface for the composition MPH_3^+ has been explored more broadly via the structures shown in Figure 5. Table S1 in the Supporting Information provides relative energies of the local minima for the composition MPH_3^+ for each of the metals and data on the magnitudes of the metal preferences. The surface has been explored further for Ru with the metal atom at different positions on and in the H_3P cone, all of which proceed via **AA**, as shown in Figure 5. The objective here was to explore transformations relating to mechanism, not necessarily to find global minima.

Correlation of Reaction Direction and Theory. There is a clear correlation between the observed experimental reaction direction, coordination or dehydrogenation, and both the calculated lowest energy structures for MPH^+ and the character of the geometry−energy hypersurface of MPH_3^+, as follows. (a) For those metals that are observed to dehydrogenate phosphane, the lowest energy structures for MPH^+ contain M−H bonding; the exceptions are Pd and Au, which are on the border of the differentiation of reaction type and are not "efficient" dehydrogenating metals. (b) Metals that are observed only to add phosphane do not contain M−H bonding in their lowest energy structures for MPH^+. (c) Similarly, barrierless migration of an H atom from P to M is calculated for the dehydrogenating metals, with the exception of Rh, Pt, and Au, which do not break P−H bonds. However, for Rh and Pt, H on M does not revert to P, Figure 6, consistent with the reaction channel. (d) The reverse H atom migration, from M to P, is calculated to be a barrierless process for the addition metals, with the exception of Cr.

Mechanism of the First Stage of Dehydrogenation. Figure 5 indicates that five metals, Mn, Nb, Mo, Hf, and Ta, are calculated to have barrierless migration of more than one H atom from P to M. This multiple H atom migration leads to an obvious intermediate for the elimination of dihydrogen, namely $(H_2)MPH^+$ or $(H_2)HMP^+$ with dihydrogen bound to M. Possible mechanisms for the first-stage loss of H_2 from MPH_3^+ are illustrated in Figure 7. Mechanisms involving loss of single H atoms are not considered, as this pathway is not experimentally significant. Mechanism III (Figure 7) is discounted (see below),

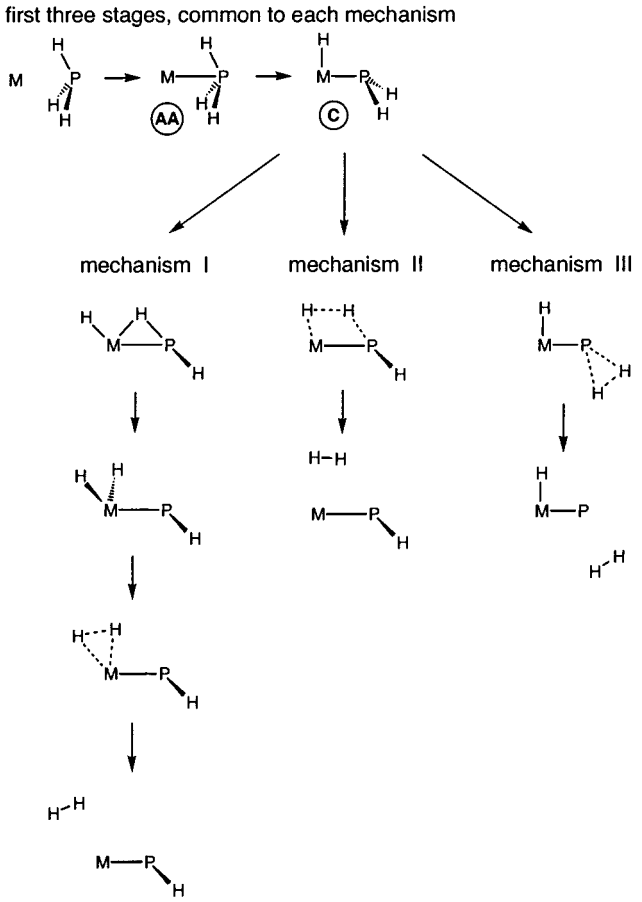

Figure 7. Possible mechanisms for the elimination of H_2 from $HMPH_2^+$.

due to a calculated high barrier against loss of H_2 from P. Mechanisms I and II involve the migration of H atoms from P to M prior to elimination and are evaluated using Ru as a representative metal.

To estimate the activation energies for individual steps in these reactions, we employed a reaction path following (RPF) transition state search technique, which is described in the section on computational methods. Gradient based transition state searches generally provided little valuable information, even close to the RPF transition state. This is due to the configurational freedom of these molecules, which is evident in the flat gradients, particularly with respect to the position of H atoms on Ru, the H−Ru−P and H−Ru−H angles, and H−Ru−P−H dihedral angles.

Figure 8 shows the calculated reaction profile for mechanism I. The initial bonding of Ru^+ to one of the hydrogen atoms results in a stabilization of ca. 10 kcal mol^{-1}. The subsequent migration of the hydrogen to the metal atom is exergonic by ca. 40 kcal mol^{-1} and results in the $HRuPH_2^+$ intermediate, **C**. The next step, the transfer of a second hydrogen from P to M, requires activation for M = Ru. To determine the activation energy, we employed an RPF search with the M−P−H angle for the migrating H atoms as the variable. The lowest energy transition state found by this method, **H** (Figure 8), lies roughly 25 kcal mol^{-1} above the $HRuPH_2^+$ intermediate. In the gas phase, the energy to overcome this barrier should be available to the molecule from the energy released by the first two steps in the mechanism, as expedient loss of this energy via collision is unlikely due to the low pressure and collision frequency. It is noted that for this mechanism to be feasible the efficiency of radiative and collisional energy loss must be low enough to allow the second H migration to occur. This is discussed further below. The next step in the mechanism requires the formation of a bond between the two H atoms bound to Ru, **J** → **K** (Figure 8). RPF searches were difficult, as the energy surface for this process was calculated to be very flat. All configurations were found to lie within 5 kcal mol^{-1} of each other, suggesting that this is a facile process. The final step involves the loss of M-bound H_2 from the molecule. Separate RPF searches were performed using both the M−H distances and the H−M−H angle as variables. The energy profile in Figure 8 reveals that the process does not involve a transition state, and hence, the behavior is not activational but dissociative. The dissociation energy associated with the loss of H_2 is calculated to be 15 kcal mol^{-1}, which is small in comparison with the exothermic portions of the mechanism.

The activation energy for the elimination of H_2 from the M−P bond in mechanism II (Figure 7) is calculated to be >50 kcal mol^{-1}. Mechanism III is unfavorable because an RPF search reveals that the activation barrier to loss of H_2 from P is 65 kcal mol^{-1}, which is more than the energy available from M^+ to PH_3 bond formation and H migration. These energy barriers are at least twice the size of the largest barrier in mechanism I. This result for mechanism III agrees with the calculated

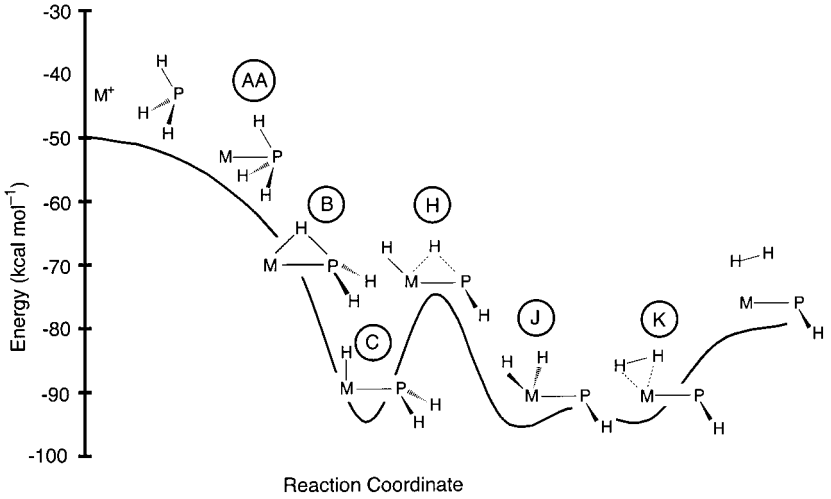

Figure 8. Calculated reaction pathway for the elimination of H_2 by reaction of Ru^+ with PH_3. The energy available from the initial coalescence is sufficient to overcome subsequent activation barriers. The reaction mechanism is further described in the text.

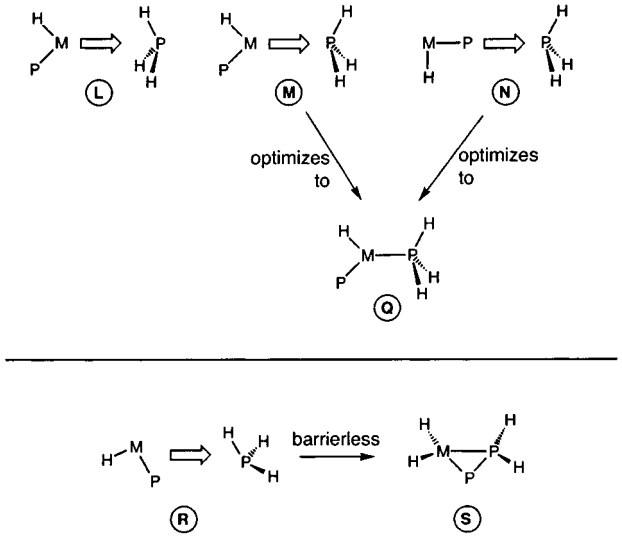

Figure 9. Approaches of HMP^+ to PH_3, and consequences during energy minimization. The approach trajectory **R** leads to the transfer of H to M and the formation of a P−P bond.

endergonicity of 65 kcal mol^{-1} for the loss of H_2 in the reaction of PH_3 with P^+,[20] and at least 40 kcal mol^{-1} for loss of H_2 in the reaction of PH_3 with PH^+.[33]

Reactions eliminating H_2 allow the loss of excess energy through the kinetic energy of the product molecules, while the mechanism of simple addition of PH_3 to M^+ must lose excess energy via collisional or radiative processes. Based on the experimental observation that dehydrogenation is substantially more efficient than addition, the efficiency of dissociative energy loss in this system must be greater than the radiative and collisional processes combined. This provides some justification for the assumption made above, that intermediates retain energy long enough to overcome activation barriers in the reaction mechanism.

Mechanism of the Second Stage of Dehydrogenation. The second stage of the dehydrogenation cycle, eq 3, was modeled in a fashion similar to the first stage. A second phosphane may approach the product of the first stage of the reaction (bent HMP^+) in a number of ways. Approach trajectories and their consequences are shown in Figure 9.

The approach trajectory **L** has negligible energy gradient. The trajectories **M** and **N** (Figure 9), in which the Ru or P of $HRuP^+$ approach the P of PH_3, lead to **Q**. The collision orientation that does lead to favorable reaction is **R** (Figure 9), in which an M−P bond of $HRuP^+$ approaches an H−P bond of PH_3. This optimizes to structure **S**, in which one H atom has transferred from P to Ru, and the P−P bond has been formed. A transition geometry for **R** → **S**, which has a P−P distance of 2.1 Å and an H−Ru distance of 2.1 Å, proceeds without barrier to **S**; the energy at this geometry is about 5 kcal mol^{-1} above separated $HRuP^+$ and PH_3, and it is probable that there is a lower or absent barrier for **R** → **S**. The next step would be the elimination of H_2 from the Ru center, followed by transfer of the remaining two H atoms to the Ru, and finally the loss of the remaining dihydrogen, leaving RuP_2^+; this part of the mechanism is considered to be similar to the H transfer and H_2 elimination of Figure 8.

We briefly consider the processes, intermediates, and products after the first cycle of eqs 2 and 3. As is evident in Table 1, the ions observed for the metals Ru, Rh, Hf, Ta, W, Os, Ir, and Pt are only those of the dehydrogenation cycles of eqs 2′ and 3′, with no more than one H atom in any stable product. For these metals, complete elimination of H_2 continues to be facile during each cycle of reactions 2′ and 3′. However, in contrast, the continuing dehydrogenation effected by the metals Nb and Mo yields series of products containing more than one H atom (for example $[MoP_7H_5]^+$), and a number of metals form MP_2H_2 and MP_4H_2 that are not consistent with (2′) and (3′) only. Molybdenum forms a rich set of eight H-containing products not accounted for by eqs 2′ and 3′.

An obvious hypothesis for the occurrence of these hydrogenated products is that the decreasing accessibility of metal coordination sites in later cycles causes H atoms to be trapped on bound P atoms and unable to transfer to M to allow M-mediated formation of H−H bonds and H_2 elimination. However, this raises the concomitant question of the structure of the phosphorus coordination in the later products, such as MP_6^+, MP_7H^+, and MP_8^+, formed by the cycles of complete dehydrogenation. In both cases, it is possible and indeed probable that there is M-mediated P−P bond formation and coordination by P_3, P_4, and larger P_n moieties. These are well known in species characterized in condensed phases.[34] Such aggregation of P atoms increases the coordinative space and opportunities for H_2 elimination at M. Detailed density functional calculations on the species $[MoP_3H]^+$, $[MoP_3H_3]^+$, $[MoP_4]^+$, $[MoP_4H_2]^+$, $[MoP_6]^+$, $[MoP_6H_2]^+$, $[MoP_6H_4]^+$, $[MoP_8]^+$, and $[MoP_8H_4]^+$, to be reported separately, support these general hypotheses.

Metal Dependence of Reaction Energies. The preceding discussion has focused on mechanisms and calculated structures of intermediates and transition states for the reactions. A fundamental question concerns the properties (or combinations of properties) of the metal ions M^+ that determine the reaction type variation and the pattern in Figure 3. Neither the first nor second ionization potential of the metals (or their difference), or the cation radii of the metals, correlate with the differentiation of addition and dehydrogenation reactions. A more subtle electronic, thermodynamic, or kinetic property of each metal is more likely to be the cause of the reactivity differences. In an attempt to answer this question, we made a comparative analysis of the energies of the first influential stages of the reactions.

Figure 10 (a) plots the difference in energy between the first products of the two reaction pathways as defined in eqs 1 and 2, that is, the difference E {H_2 plus the most stable HMP^+ structure for each M} − E {addition structure MPH_3^+}. This difference provides a direct comparison of thermodynamic stability between the two pathways for the various metals; a positive value indicates thermodynamic favorability of coordinative addition, eq 1. A pattern evident in Figure 10 (a) is that metals toward the right of all three transition metal series show an increased favorability for the adduct structure that contains no M−H bonds. This calculated trend reflects the observed behavior, and if a horizontal line is drawn at 45 kcal mol^{-1} in Figure 10 (a), then the metals are separated into groups that match the experimental behavior separation. Notice that the behavior of Cr, apparently anomalous in Figure 3, is explained

(33) Antoniotti, P.; Operti, L.; Rabezzana, R.; Tonachini, G.; Vaglio, G. A. *J. Chem. Phys.* **1998**, *109*, 10853−10863.

(34) (a) Di Vaira, M.; Sacconi, L. *Angew. Chem., Int. Ed. Engl.* **1982**, *21*, 330−342. (b) von Schnering, H. G.; Hönle, W. *Chem. Rev.* **1988**, *88*, 243−273. (c) Scherer, O. J. *Angew. Chem., Int. Ed. Engl.* **1990**, *29*, 1104−1122. (d) Whitmire, K. H. *Adv. Organomet. Chem.* **1998**, *42*, 1−145. (e) Scherer, O. J.; Weigel, S.; Wolmershauser, G. *Chem. Eur. J.* **1998**, *4*, 1910−1916. (f) Scherer, O. J.; Ehses, M.; Wolmershauser, G. *Angew. Chem., Int. Ed. Engl.* **1998**, *37*, 507−510. (g) Scherer, O. J. *Acc. Chem. Res.* **1999**, *32*, 751−762.

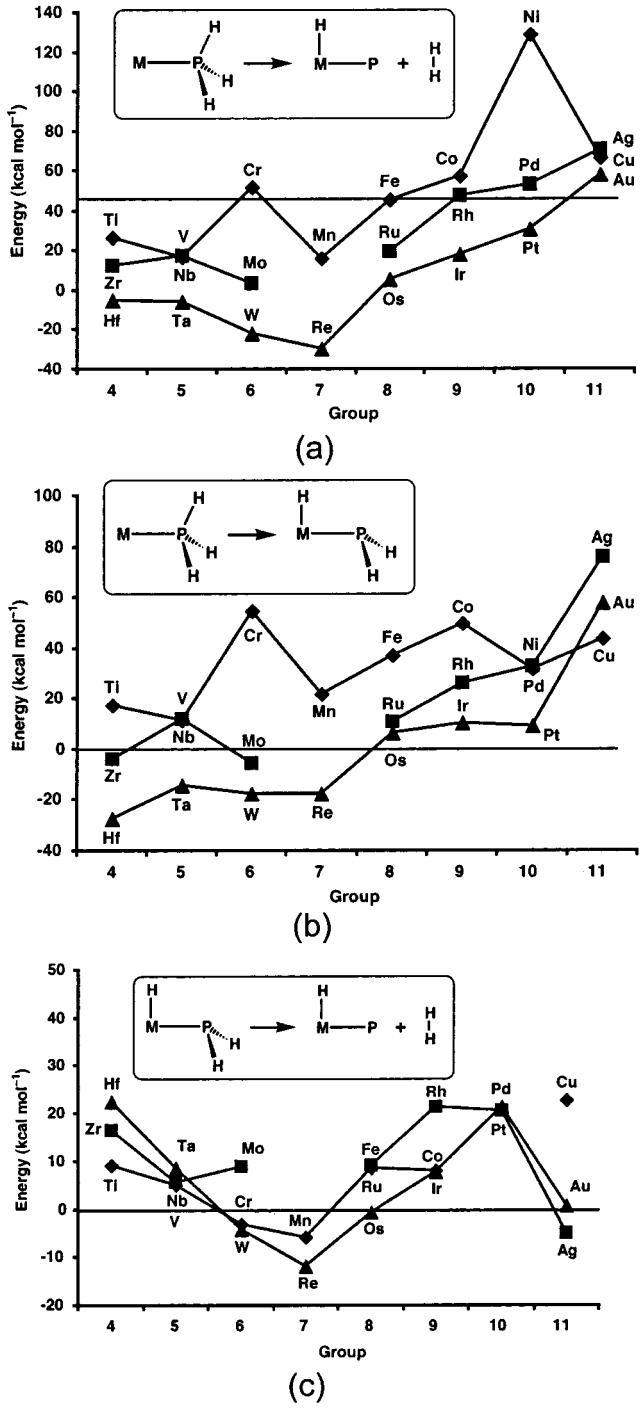

Figure 10. Metal dependence of reaction energies. (a) A plot of the calculated energy difference between the products of the two observed reaction pathways, i.e., addition versus dehydrogenation, eq 1 versus eq 2. The energy is calculated as E {H_2 plus the most stable HMP^+ structure for each M (see Table 4)} − E {adduct MPH_3^+}. More positive values favor the addition pathway. The horizontal line separates the metals observed to undergo addition (above) and those undergoing dehydrogenation (below). (b) A plot of the calculated energy difference for the rearrangement shown, calculated as E {H−M−PH_2^+ structure (structure C Figure 5), the H−M−P angle is constrained to 90° for those metals where this structure is not a minimum)} − E {adduct MPH_3^+}. More positive values favor the adduct MPH_3^+. (c) A plot of the calculated binding energy difference for the dissociation shown, calculated as E { the most stable HMP^+ structure (as shown in Table 4) plus the binding energy of H_2} − E { H−M−PH_2^+ (structure C Figure 5), the H−M−P angle is constrained to 90° for those metals where this structure is not a minimum)}.

nicely by the data in Figure 10 (a). The correlation of the data in Figure 10 (a) and observed reaction channels lead to the conclusion that thermodynamic stability of products plays a major role in determination of the reaction pathway for $M^+_{(g)} + PH_{3(g)}$.

While the addition pathway is likely to be single stage, dehydrogenation consists of several steps, as illustrated in Figure 8. Figure 10 (b) plots the net stabilization for the transfer of one H atom from P to M, involving the formation of an M−H bond and breaking of one P−H bond. The plot is very similar to that of Figure 10 (a) and is similarly consistent with the experimental observations, suggesting that the determination of reaction pathway depends strongly on the extent to which the transfer of the first H atom is exergonic. Figure 10 (c) plots change in binding energy for the remainder of the dehydrogenation process. The energy changes are smaller than those for the initial H atom transfer step ($\leq$25 kcal mol^{-1} for Figure 10 (c) versus $\leq$80 kcal mol^{-1} in Figure 10 (b)), and the energy changes do not track the observed metal dependence of reaction type. Therefore, the energy of the initial H atom transfer is the primary factor in the determination of reaction pathway.

Discussion and Summary

Two of the reactions reported here, with Cr^+,[17] and Pt^+,[19] were investigated recently by Schwarz and co-workers. With Cr^+, they and we both observe only $CrPH_3^+$. With Pt^+, they saw one further stage of dehydrogenation, to PtP_6^+, and measured rate constants. On the basis of the CID for PtP_2^+, PtP_4^+, and PtP_6^+, and the addition reactions of PtP_2^+ and PtP_4^+ but not PtP_6^+ with benzene, they concluded that these products contain P_2 units and that PtP_4^+ and PtP_6^+ have pseudo-tetrahedral and pseudo-octahedral structures, respectively. Our calculations, for molybdenum, suggest that P−P bond formation is likely to be prevalent in the latter stages.

We can compare the dehydrogenation of PH_3 by M^+ with similar reactions of P^+ and PH^+ with PH_3.[20,33] In all three cases, loss of H_2 is more favorable than loss of H. The calculated reaction and transition energies are in the order $Ru^+ < PH^+ < P^+$, which is consistent with the concept of a softer metal ion. This also agrees with our calculations that elimination of H_2 from P in $HRuPH_2^+$ requires greater activation energy than elimination of H_2 from Ru after rearrangement to H_2RuPH^+.

For the first time the reaction of PH_3 with metal ions in the gas phase has been investigated comparatively for most of the transition metals. Addition and dehydrogenation reaction pathways occur, largely as metal-dependent separate channels, with few instances of crossover between the channels. Both reaction types can recur sequentially, leading to adducts up to $M(PH_3)_4^+$ (for Cu), and to MP_mH^+ (m odd) and MP_n^+ (n even). The largest number of dehydrogenation cycles, nine, occurs for Os, and most metals which dehydrogenate do so for at least five cycles. Dehydrogenation is generally at least an order of magnitude faster than addition, and the fastest dehydrogenating metal ion, Zr^+, is believed to react at close to the collision rate.

Density functional calculations have reproduced and elucidated the broad range of experimental behavior. By exploration of geometry−energy surfaces for collision trajectories, we detected the principal differences between encounters leading to MPH_3^+ with metal bound only at P and encounters in which at least one H atom migrates from P to M as a first intermediate for dehydrogenation. This PH → MH migration is a facile process for many metals. The full reaction profile for the first elimination of H_2 has been described in the case of Ru^+, with the conclusion that the energy released in the early stages

involving the transfer of the first H from P to Ru is sufficient to activate the migration of the second H atom and the dissociation of H_2 from Ru. Dissociative energy loss favors the dehydrogenation reaction and accounts for its observed efficiency relative to coordinative addition. The energetic origins of the metal influence on reaction type have been traced to the energy changes for the first stage migration of H from P to M.

These experimental and theoretical results will be valuable in applications where $PH_{3(g)}$ is used in the generation of bulk and surface materials involving metal phosphides. Facile elimination of H_2 is a requirement of such processes and is influenced by the identity of the metal. We have shown that a considerable number of the transition metals, as gaseous monocations, efficiently generate metal phosphides by reaction with $PH_{3(g)}$. The composition of the resulting metal phosphide can also be influenced by the identity of the metal, and the results reported here indicate that phosphorus rich species can be generated with excess PH_3. Phosphorus rich cations $MP_n^+{}_{(g)}$ (n even) and a variety of anions $M_xP_y^-{}_{(g)}$ have also been generated by laser ablation of solid MP (Co and Ni) and solid mixtures of M and P_4.[26d,35]

Acknowledgment. This research is supported by the Australian Research Council and the University of New South Wales. Hugh Harris acknowledges the award of an Australian Postgraduate Scholarship.

Note Added after ASAP. The version of this article that was posted on the Web on November 17, 2001, did not contain a description of the Supporting Information available. A description is present in the version posted on December 26, 2001.

Supporting Information Available: Tables S1−3. This material is available free of charge via the Internet at http://pubs.acs.org.

IC0105821

(35) Yi, M.; Fisher, K.; Dance, I. G. *New J. Chem.* **2001**, *25*, 73−82.